JGR Oceans

RESEARCH ARTICLE
10.1029/2020JC016881

Postbomb Subtropical North Pacific Surface Water Radiocarbon History

Thomas P. Guilderson[1], Daniel P. Schrag[2], Ellen R. M. Druffel[3], and Ron W. Reimer[4]

[1]Ocean Sciences Department, University of California, Santa Cruz, CA, USA, [2]Department of Earth and Planetary Sciences, Harvard University, Cambridge, MA, USA, [3]Department of Earth System Science, University of California, Irvine, CA, USA, [4]CHRONO Centre, Queen's University, Belfast, UK

Key Points:

- The Δ14C record contains ENSO variability reflecting the lateral advection of low latitude surface waters driven by Sverdrup dynamics
- Prebomb (1947–1954) values average −55‰; ±1 (SEM) with a seasonal cycle: Less positive during winter and more positive during summer
- A 1D diffusion model forced with local/regional conditions cannot recreate the surface water ^{14}C record

Supporting Information:

- Supporting Information S1
- Data Set S1

Correspondence to:
T. P. Guilderson,
tguilder@ucsc.edu

Citation:
Guilderson, T. P., Schrag, D. P., Druffel, E. R. M., & Reimer, R. W. (2021). Postbomb subtropical North Pacific surface water radiocarbon history. *Journal of Geophysical Research: Oceans*, *126*, e2020JC016881. https://doi.org/10.1029/2020JC016881

Received 10 OCT 2020
Accepted 11 JAN 2021

Abstract We have generated a high-resolution coral $\Delta^{14}C$ record from the leeward side of the Big Island of Hawai'i in the subtropical North Pacific. The record spans 1947–1992, when the coral was collected, and includes a brief prebomb interval as well as the postbomb era. Mean prebomb (1947–1954) values average −55‰ (±1, SE of the mean) with a clear seasonal cycle. Values are less positive during winter when vertical exchange mixes surface and lower-^{14}C subsurface waters. The postbomb annual maximum occurs in 1971 (+160‰) and decreases in a series of shifts to +105‰ in 1991, the end of our coral-based reconstruction. The decrease is not monotonic and has inflection points during the La Niña years of 1973, 1977, and 1984. Imbedded in the $\Delta^{14}C$ record is interannual variability in the El Nino-Southern Oscillation band which is interpreted to reflect the lateral advection of low latitude surface waters as part of the oceanic Hadley Cell driven by Sverdrup dynamics.

Plain Language Summary We have reconstructed the radiocarbon content of North Pacific Gyre (NPSG) surface waters from a reef-building coral cored off the leeward side of the Big Island of Hawaii. The record spans 1947-1992, capturing the full pre/post-bomb transition. The post-bomb maximum occurred in 1971. The record documents seasonal and inter-annual variability in surface water processes: lateral exchange and cross thermocline exchange. Local to regional wind-forcing is not sufficient to recreate the pre/post-bomb peak in a simple 1-D box diffusion model. One possible implication of this observation is there is a strong influence of waters recirculated within the NPSG on the radiocarbon content of surface gyre waters.

1. Introduction

In a zonally averaged and simplified sense, there exists an upper oceanic Hadley Cell in the Pacific: during the winter season subduction occurs in the subtropics and extra-tropics and this water ventilates the tropical thermocline where it upwells and returns to the subducting regions through surface flow (e.g., Wyrtki & Kilonsky, 1984). Significant interior pycnocline exchange occurs between the subtropics and tropical thermocline (Johnson & McPhaden, 1999). Building on the observational evidence of Deser et al., (1996), it has been hypothesized that temperature anomalies originating at the sea-surface in the subtropics can be propagated via this subsurface pathway and interact with the equatorial thermocline, changing the character and sensitivity of the El Niño- Southern Oscillation (ENSO) (Gu & Philander, 1997; Zhang et al., 1998). Tritium and ^{3}He tracer data indicate that the ventilation time-scale of the tropical thermocline is on the order of decades (Fine et al., 2001; Jenkins, 1996). It is therefore a logical extension to hypothesize that the intergyre exchange between the extra-tropical subduction zones and the tropical thermocline could determine the decadal-scale climate character of the tropical Pacific (Gu & Philander, 1997), as well as other important processes.

Follows et al. (2002) and subsequently Ito and Follows (2003) convincingly promote the concept that solubility and ventilation of the subtropical thermocline has the potential to impact the concentration of atmospheric carbon dioxide (CO_2). In their studies where they explored the relationship between ocean dynamics and atmospheric CO_2, through a series of scaling arguments and idealized abiotic ocean circulation model experiments, they came to the conclusion that the sensitivity of atmospheric pCO_2 to wind-forcing is dominated by the ventilation of the subtropical thermocline. They specifically predict up to 30 ppmv variations in atmospheric pCO_2 (referenced to 369ppm) directly attributable to the subtropics under reasonable

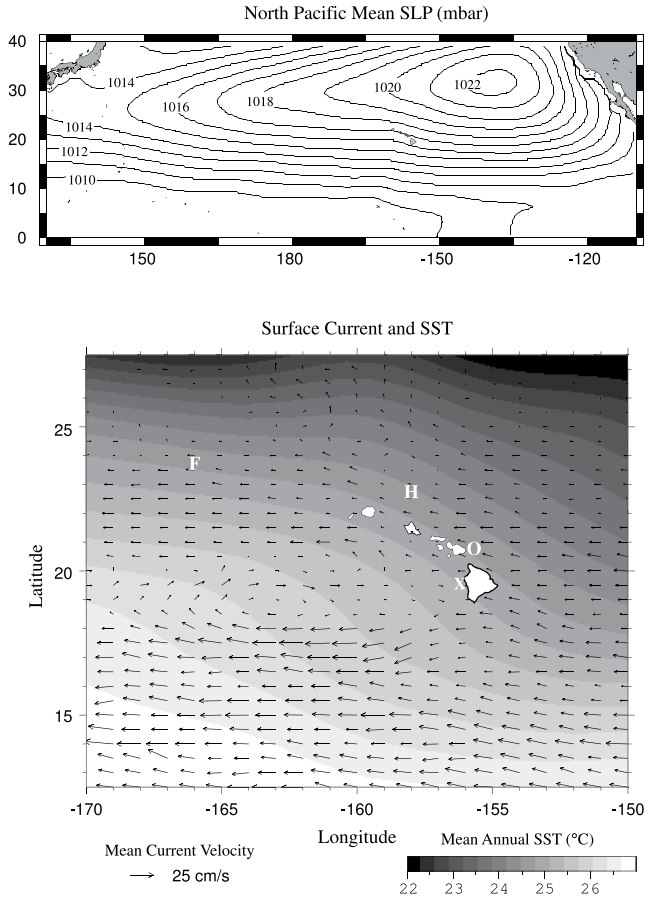

Figure 1. Regional North Pacific sea level pressure (mbars) showing the position of the North Pacific subtropical gyre (~32°N 135°W) and (b) mean annual sea surface temperature and surface currents as compiled from drifter data (after Flament, 1996). The location of the coral recovered off the Big Island is denoted with an "X" whereas other Hawai'ian locations discussed in the text are: Oahu ("O"), HOT Station Aloha ("H"), and French Frigate Shoals ("F").

variations in wind speed and diapycnal mixing rates. The importance of subtropical waters and their role in the uptake and redistribution of CO_2 has been subsequently confirmed by direct estimates of the uptake of anthropogenic carbon through the WOCE/CLIVAR/GOSHIP era (e.g., Iudicone et al., 2016). It follows that accurate modeling of subtropical dynamics and air-sea exchange may be relevant in predicting future atmospheric pCO_2 on multidecadal timescales; the time-scale apportioned to intergyre exchange between the subtropics and the ventilated tropical thermocline.

Large-scale global ocean general circulation models (OGCM) and coupled carbon climate models are used to estimate the uptake and redistribution of anthropogenic carbon. Although there are demonstrable biases in the interior circulation (e.g., Doney et al., 2004; Graven et al., 2012), in general the range of globally integrated uptake of anthropogenic CO_2 in these OGCMs is small (e.g., Khatiwala et al., 2013; Matsumoto et al., 2004; Orr et al., 2001). Simply, although the global mean uptake is consistent among many models, the geographical distribution of uptake (including amount) and redistribution (penetration) are not.

The time history of the ocean's uptake and redistribution of atmospheric nuclear weapons testing, or bomb $^{14}CO_2$ is a diagnostic of local and large-scale processes. The immediate postbomb rise in surface $\Delta^{14}C$ is a unique diagnostic of air-sea CO_2 exchange (e.g., Guilderson et al., 2000; Mahadevan, 2001, among many) and the uptake of bomb^{14}C has been used to infer air-sea CO_2 exchange rates (e.g., Broecker & Peng, 1982; Sweeney et al., 2007; Wanninkhof, 1992). The initial rise has been used, for example, in establishing a variety of biological chronologies (e.g., Kerr et al., 2005). OGCMs that include radiocarbon have had difficulty in reconstructing the observed prepost bomb amplitude in the subtropics (Guilderson et al., 2000; Rodgers et al., 2000; Toggweiler et al., 1989, among others). In these large-scale OGCMs the prepost bomb amplitude is often too large and occurs earlier than observations, implying that in these models the surface waters are not being mixed well enough with, and into, waters below. A corollary to this is an inference that the penetration of both heat and anthropogenic CO_2 could be being slowed down or trapped in surface waters in these models.

In this study, we take advantage of the fact that the uptake and redistribution of bomb-^{14}C is a sensitive indicator of air-sea exchange and mixing processes (e.g., Duffy et al., 1995; Toggweiler et al., 1991). Subannual radiocarbon (^{14}C) measurements derived from coral skeletal material, which accurately records $\Delta^{14}C$ of the total dissolved inorganic carbon (DIC), have added to our knowledge of the general shallow circulation of the Pacific (e.g., Druffel, 1987; Druffel et al., 2014; Guilderson et al. 1998; Moore et al., 1997). To further elucidate the processes that influence these waters, we have reconstructed the $\Delta^{14}C$ variability of North Pacific Subtropical Gyre (NPSG) surface waters. We have done this via a ~bimonthly resolved $\Delta^{14}C$ record from a coral recovered from the western side of the Big Island of Hawai'i.

2. Site Location and Oceanography

The main islands of the Hawai'ian archipelago span 2.5° of latitude from the Big Island of Hawai'i (~19.5°N) to the islands of Kauai and Nihau (~22°N) in an arc between 155 and 160°W (Figure 1). Regionally, sea surface temperatures (SST) average ~25.3°C with minima of ~24°C occurring during February/March, and maxima of ~27 in September (Flament, 1996; Rayner et al., 1996). In the gyre, evaporation exceeds precipitation except around the islands where island induced and orographic precipitation occurs (e.g., Chu & Chen, 2005; Diaz & Giambelluca, 2012; O'Connor et al., 2015). Mean surface salinity is ~34.9 psu and

ranges seasonally ~0.5 psu with slightly greater interannual variability as monitored at the HOT-ALOHA site (Bingham & Lukas, 1996; cf., http://hahana.soest.hawaii.edu/hot/hot-dogs/). Climatological mixed layer depths for the 19.5°N/155.5°W grid box as defined by the 0.125 density criterion average 40 m from a March low of 28 m to a November maximum of 49m (Monterey & Levitus, 1997, and subsequent updates). We note that the WOA (World Ocean Atlas) product mean is slightly shallower (45 vs. 60 m) for the equivalent gridbox containing the HOT-ALOHA (22.5°N/158°W) station data (n = 4,218 casts). If using a smaller density criteria, such as proposed for Argo float products (e.g., Holte & Talley, 2009), the defined mixed layer depth will be shallower. From the climatological data one can infer that local winter mixing and subduction produces waters with densities approaching a potential density of 25.0 kg-m^{-3}. The region is dominated by the northeasterly trade winds (averaging ~7.5 m/s) associated with the North Pacific anticyclone. There is a slight seasonal cycle to the wind field in conjunction with the northward migration of the gyre during boreal summer (DaSilva et al., 1994). The large-scale surface circulation is dominated by the clockwise gyre circulation with mean currents near Hawai'i coming from the east-southeast. To the south of Hawai'i is the North Equatorial Current (NEC) whose velocity decreases as it approaches the islands. Locally, the NEC has less seasonal variability than up and downstream, but in general has larger velocities during November–March and lower velocities during spring-summer (Laurindo et al., 2017; Lumpkin & Johnson, 2013). The NEC bifurcates at the Big Island of Hawai'i where the northern branch becomes the North Hawai'ian Ridge Current and the southern branch continues westward as the NEC. Two circulation features appear to the west, in the lee of the main islands: a counter-clockwise circulation nominally at ~20.5°N and a clockwise "cell" centered at ~19°N which merges with the southern branch of the NEC (Flament, 1996; Lumpkin & Johnson, 2013; Yoshida et al., 2010). The large scale mean circulation is complicated by two regionally important processes affecting surface water characteristics. The first is the interaction of the NEC with the Big Island of Hawai'i where numerous eddies are shed off its southernmost points of Ka Lae and Kauna Point. The second is shear zones which are set-up in the lee of the islands in the main channels between the islands. The shear between the faster and slower wind fields in combination with the Coriolis force yields divergent motion (upwelling) at the northern shear line and convergent motion (downwelling) at the southern boundary of the individual channels (e.g., Bidigare et al., 2003).

3. Analytical Methods

A large (6.8 m) *Porites lobata* coral head at 8 m bottom depth, located 2.5 km south of Keauhou Bay (nominally at 19.5621°N, 155.9622°W) in the Kona District, and 50 m from shore on the western side of the Big Island of Hawai'i was cored in April of 1992. The cores (~5 cm diameter) were cut into ~1 cm slabs, cleaned in distilled water, and air-dried. X-radiographs were taken to identify the major vertical growth axis, and document density variations. The coral was sequentially sampled, using a 2 mm spherical bur, along the main vertical growth axis to obtain ~10 mg of material. The coral slab was mechanically advanced under the drill in 1 mm increments. Splits (~1 mg) were reacted in vacuo in a modified common acid-bath autocarbonate device at 90°C and the purified CO_2 analyzed on a gas source stable isotope ratio mass spectrometer. Analytical precision based on an in-house standard is better than ±0.05‰ (1σ) for both oxygen and carbon relative to Vienna Pee Dee Belemnite (Coplen, 1993). Consistent with other published coral stable isotope data we do not use the aragonite acid-alpha, but that of calcite. Strontium to calcium ratios were determined on ~1 mg splits using an inductively coupled plasma atomic emission spectrometer (ICP-AES) following the methodology of Schrag (1999). Analytical precision based on an in-house homogenized coral standard is ±0.2% (Schrag, 1999).

Chronologies of hermatypic-reef building corals rely upon the presence of annual density band couplets (e.g., Dodge et al., 1980) or the seasonal variability in coral $\delta^{13}C$ that primarily reflects surface irradiance (e.g., Fairbanks & Dodge, 1979; Grottoli, 1999; McConnaughey et al., 1997; Shen et al., 1992). Independent chronologies based on these two methods on the same coral specimen tend to agree within a few to 6 months (e.g., Shen et al., 1992). Although variable, rainfall data for the Main Hawaiian Islands, including the low elevation stations in the lee of the Big Island, document June-July as the putative dry season (Chu & Chen, 2005; Diaz & Giambelluca, 2012**)** when the coral skeleton $\delta^{13}C$ should have more positive $\delta^{13}C$ values, and December-January as the wettest months. Splicing of individual transects was accomplished via comparison of the geochemical data, ultimately including ^{14}C, in concert with the x-radiographs. We created a

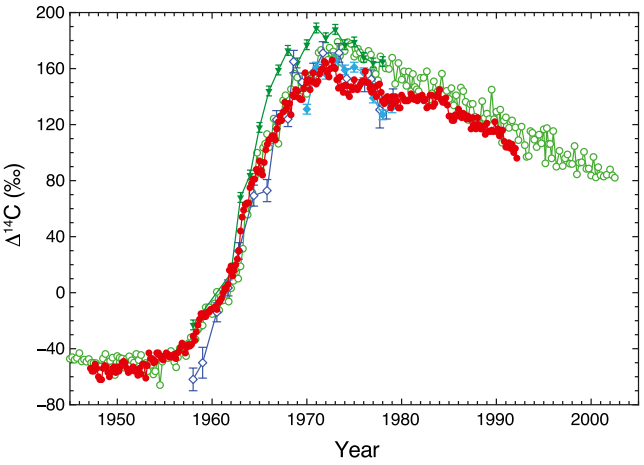

Figure 2. $\Delta^{14}C$ in corals from the Hawai'ian archipelago. Records shown include that of the Big Island of Hawai'i (solid red circles, this study), French Frigate Shoals (inverted green triangles, Druffel, 1987), and two independent records from Oahu (filled blue diamonds, Druffel, 1987; open blue diamonds, Toggweiler et al., 1991). Also plotted is a coral reconstruction from Kure Atoll (open green circles, 28.4°N, 178.3°W; Andrews et al., 2016), also within the subtropical gyre and ~2,500 km to the northwest of the Hawai'i.

preliminary age model based on the seasonal structure within the $\delta^{13}C$ record and visible stratigraphy but because we were not interested in the coral $\delta^{18}O$ and Sr/Ca as an independent measure of temperature, we have refined our age model by first checking the age-model against anticipated seasonal $\delta^{18}O$ maxima with coolest temperatures (Mar/Apr) and minima with warmest temperatures (Sept/Oct). The final age model used a comparison of coral Sr/Ca with instrumental records. To achieve this, we took our stable isotope/sclerochronology age-model and filtered the Sr/Ca record to extract the annual component. The filtered record was then optimized by aligning the peaks and troughs reflecting seasonal sea surface temperature variations to the 1° × 1° resolution GOSTA v2. (Rayner et al., 1996) reconstructed SST (1903–1994) for the equivalent grid box (19.5°N 156.5°W) containing the coral. The average difference between the stable isotope/sclerochronology age-model and the Sr/Ca optimized model was 0.1 ± 0.002 (standard error of the mean, SEM) year. Between the tie-points reflecting seasonal maximum and minimum temperatures (nominally Sept/Oct and Mar/Apr respectively) the refined or tuned age-model has an estimated error of ±1.5 months. The implied linear extension rate averages 13.4 ± 2.7 mm/yr and varies between 9 and 21 mm/yr (Supporting Information S1).

For radiocarbon, we analyzed every sample to 130 mm (composite depth) and every other sample, that is, every other milimeter, to 604 mm. Splits (~8 mg) were acidified in vacuo at 90°C and the evolved purified CO_2 converted to graphite in the presence of cobalt catalyst (Vogel et al., 1987). Radiocarbon results are reported as $F^{14}C$ (Reimer et al., 2004) and age-corrected $\Delta^{14}C$ (‰) as defined by Stuiver and Polach (1977) both of which include the $\delta^{13}C$ correction obtained from the stable isotope results, and a background correction based on ^{14}C-free calcite ($F^{14}C = 0.0016 \pm 0.0004$, $n = 25$). Precision and accuracy of the radiocarbon measurements is ±4‰ (1σ) as monitored with an in-house homogenized coral standard ($F^{14}C$ 0.9443 ± 0.0041, $n = 48$) and officially distributed secondary and tertiary radiocarbon standards. For overlapping transects, the end or start of the transect was trimmed back to the nearest chronological tie-point. Overlapping transect ^{14}C data were averaged and the complete record linearly interpolated to bimonthly resolution in the time-domain.

4. Results

The age model for this coral deviates slightly from the prebomb era study of Druffel et al., (2001). With the addition of continuous subannual ^{14}C data, a small offset associated with the transition between two subcores (transect D and transect E) was determined (Supporting Information S1). For these two subcores, there were two different ways to physically match the two subcores. Unlike banding or the seasonal cycle in stable isotopes, with the ^{14}C data that exhibited a 20‰ range, we were able to resolve the binary physical match. From collection to 1981.37 the $\Delta^{14}C$ mean sample timestep is 0.07 (±0.003 SEM) year, or monthly, and 0.14 (±0.003 SEM) year, or bimonthly, for the remainder of the record. On average, each $\Delta^{14}C$ data point encompasses a month in time. Between 1947 and 1992 the coral $\Delta^{14}C$ record has a dynamic range of 232‰, from a low of −65‰ (1953.0) to a high of +167‰ (1972.7) (Figure 2). Mean annual prebomb values are approximately −55‰ (−56‰ to −52‰), similar to values reported by Druffel et al., (2001). $\Delta^{14}C$ values rise slightly in 1952 (−49‰) and again in 1953/1954 (−45‰). The mean annual value in 1955 is −42‰ and continues to rise monotonically until 1971 with the mean annual value peaking at 160‰ in 1972. The steepest rise is observed between 1961 and 1963. During this time of rising $\Delta^{14}C$ values, there is a nearly regular decrease in $\Delta^{14}C$ during late-fall and winter implying vertical mixing with subsurface waters that do not contain as much bomb-derived ^{14}C. Since the postbomb maxima, values have decreased to 100‰ in 1992. The decrease has not been consistently monotonic with shifts toward lower values occurring in 1973, 1977, and again in 1984. Post 1985 values decreased in a more monotonic way.

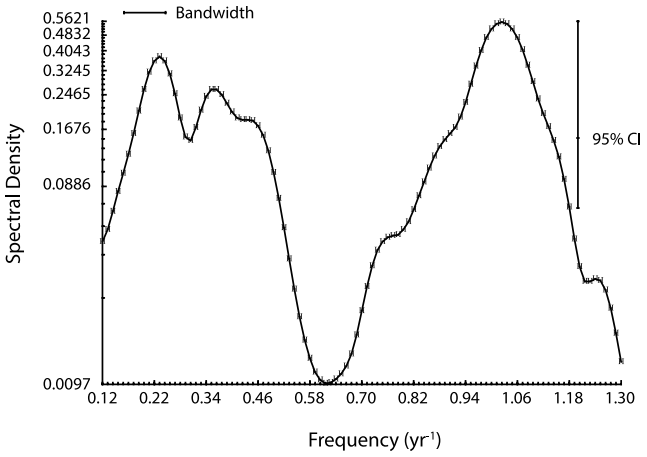

Figure 3. Frequency versus spectral density (linear-log axis) as determined via the one-third lagged autocovariance function using the "Arand" package on the high-pass filtered and smoothed Big Island $\Delta^{14}C$ record. Note the strong annual and ENSO frequencies. ENSO, El Niño-Southern Oscillation.

5. Discussion

5.1. Comparison to Other NPSG Time-Series

We compare our ~bimonthly record to coarse annual/biannual samples analyzed via traditional counting methods (Druffel, 1987; Toggweiler et al., 1991) and a quarterly resolved record from Kure Atoll (Andrews et al. 2016), nearly 2,500 km to the northwest of the Big Island at the end of the Northwest Hawaiian Island Chain. There is more than a general correspondence in the shape and amplitude of the pre/postbomb transition signal (Figure 2). The postbomb maxima at French Frigate Shoals (24°N, 166°W) is ~25‰ higher than that observed in our record. French Frigate Shoals is within or north of the intersection between the westward flowing Hawaii Lee Current, an extension of the NEC, and the eastward flowing subtropical counter current (Robinson, 1969; Yoshida et al., 2010). Therefore, it is more isolated and should, in some sense, be protected from the impact of advected lower ^{14}C water transported from the tropical North Pacific associated with the NEC. Additionally, the Big Island record may be influenced by the wind-induced, semi-permanent mesoscale anticyclonic eddy centered at ~19°N and the production of cold core eddies off the Hawai'ian Islands: processes that are known to entrain subsurface water. These dynamic processes would have the net effect of reducing the pre- to postbomb amplitude in the Big Island $\Delta^{14}C$ record. It is interesting that, although physically farther within the gyre, Kure Atoll's postbomb peak is less than that of French Frigate Shoals. The dampening may be due to local, fine-scale circulation and mixing around the atoll associated with energetic wave dynamics (Gove et al., 2013) and potential dampening due to lateral advection of lower $\Delta^{14}C$ surface water via cold water eddies from, or meanders of, the Kuroshio extension (Qiu, 2002).

5.2. Lateral Surface Water Exchange on Interannual Timescales

To quantify the interannual variability we have filtered the long-term bomb transient out of the record by passing the record through a 5-weight Tukey-cosine high pass filter with a half-width of 10 years. We then passed this record through a nine point moving average filter and determined the spectral character via the transformation of the one-third lagged autocovariance function. In addition to a strong annual cycle the record contains significant interannual power in the ENSO band (Figure 3). The interannual frequencies' significance and power is insensitive to prespectral processing methodologies including initial $\Delta^{14}C$ data interpolation, high-pass filter structure, and smoothing interval. Indeed, spectral power at annual and 3–7 year periodicity is observed in the spectrum of the nonhigh pass filtered data. Similar periodicities are found in SST, sea level pressure, and to a lesser extent the COADS derived wind field (DaSilva et al., 1994 and subsequent updates). The large scale advected ^{14}C signal reflects the relative contribution and $\Delta^{14}C$ contents of the North Equatorial Current, which incorporates not only lower-^{14}C water from the eastern tropical north Pacific but also from the California Current System. On interannual timescales, this advected component is strongly influenced by the state of ENSO, which modulates the $\Delta^{14}C$ content in east Pacific surface waters (e.g., Brown et al., 1993; Druffel et al., 2014; Guilderson and Schrag, 1998; Ingram & Southon, 1996). Cross spectral analysis of the respective one-third lagged autocovariance functions indicate that at these frequencies the $\Delta^{14}C$ time-series and Nino-3 Index are neither coherent nor in phase (not shown). This is due to the transient tracer nature of bomb-^{14}C and, more importantly, the convolution of local and nonlocal forcing that impacts the $\Delta^{14}C$ value of gyre surface waters. After the postbomb peak, the reconstructed $\Delta^{14}C$ surface water values do not decrease monotonically but have distinct inflection points coincident with La Niña events following moderate to strong El Niños (1973, 1977, and 1984). We are confident that these decreases are a consequence of changes in the large-scale wind field and the return of North Pacific upwelling conditions and advection and mixing of lower $\Delta^{14}C$ water into the NPSG.

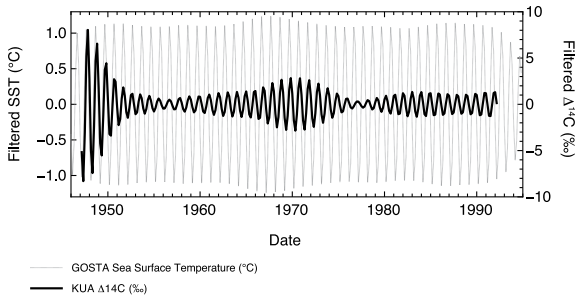

Figure 4. Seasonal $\Delta^{14}C$ variability in the Big Island coral (black solid line) relative to SST (gray dashed line) by passing the respective records through a Gaussian (1 ± 0.1 yr^{-1}) filter. The seasonal character of $\Delta^{14}C$ evolves relative to SST due to the penetration of bomb-^{14}C into the interior waters. This evolution begins as a correspondence between lower $\Delta^{14}C$ and cooler SSTs during winter mixing when vertical exchange mixes lower-^{14}C water into the surface, which, with the penetration of bomb-^{14}C into subsurface water masses, breaks down in the mid-1970s and then re-establishes itself in the 1980s. SST, sea surface temperature.

To elucidate the seasonal character of $\Delta^{14}C$ in relation to local SST, we passed both the Big Island $\Delta^{14}C$ and the GOSTA SST record through a Gaussian filter centered on 1.0 ± 0.1 yr^{-1} (Figure 4). For most of the time-series there is a regular correspondence between SST and surface water $\Delta^{14}C$ with lower $\Delta^{14}C$ and cooler winter SSTs. This correspondence appears to weaken in the late 1970s and into the1980s, when the most positive $\Delta^{14}C$ values shift toward cooler SSTs (Figure 4). Although is most likely the result of the penetration of bomb-^{14}C into the subsurface, which weakens the vertical $\Delta^{14}C$ gradient and where the redistribution of bomb-^{14}C over time leads to the highest $\Delta^{14}C$ values to be in subsurface subtropical mode waters (cf., Figure 6, Key et al., 1996; Quay et al., 1983), we recognize that the sample and age-model resolution may preclude a clearly definitive interpretation.

The Kure Atoll quarterly resolved $\Delta^{14}C$ record also contains power at ENSO and annual periodicities: over its entire length (1939–2002) as well as the interval (1947–1992) common with our Big Island record (not shown). Analysis of similarly high-pass filtered and smoothed data for the two locations has the highest cross-correlation with an offset of 0.5 year, with the Big Island leading Kure Atoll. During the prebomb era, the Kure record's relationship with local SST is opposite that of the Big Island: with lowest $\Delta^{14}C$ commensurate with high local SST. This implies that the ^{14}C signal is an advected feature and not sensu strictu a reflection of local mixing with (cooler, lower $\Delta^{14}C$) subsurface water. For the postbomb era, Kure $\Delta^{14}C$ and local SST is almost always in phase (cooler SST and lower $\Delta^{14}C$ values). At interannual periodicities the relationship between Kure and the Big Island $\Delta^{14}C$ records is complicated; in the 1970s they are not in phase, whereas in the 1980s they are more in phase. This indicates, and consistent with its much more distal location in the NPSG, that the Kure Atoll $\Delta^{14}C$ record is not simply the downstream expression of $\Delta^{14}C$ variability brought in from the NEC.

5.3. Air-Sea $^{14}CO_2$ Exchange and the Pre/postbomb Transition

There is a rich literature exploring the response of the ocean to atmospheric $\Delta^{14}C$ in 1-D box diffusion models (e.g., Chakraborty et al., 1994; Fallon et al., 2003; Mahadevan, 2001; Oeschger et al., 1975; Stuiver et al., 1983; Stuiver et al., 1986). Building on these previous studies, we place our observations in the context of local to regional and global forcing. The box-model is based on that of Oeschger et al. (1975) and used by Stuiver et al., (1983, 1986) and Reimer et al. (2013) to predict the global ocean's response to atmospheric $\Delta^{14}C$ forcing. We refer to this model as "SQO" (Stuiver, Quay, and Östlund). This model has two knobs that over longer times can play off of each other: air-sea CO_2 exchange (G, moles-m^{-2}-yr^{-1}) and ocean vertical diffusivity (K_z, m^2-yr^{-1}). A constraint on the long-term integration of G and K_z is the average $\Delta^{14}C$ value of the deep-ocean, a constraint often simplified by meeting the deep-Pacific value as measured during GEOSECS (−190‰: Östlund & Stuiver, 1980). It is useful to reinforce that because this is a 1-D model, lateral exchange and recirculation are not included. Thus, we should not expect to capture and reconstruct the full postbomb era surface water history. Additionally, there are implicit assumptions in the isotopic exchange functionalized using a piston velocity. Our primary focus are the decades on either side of the 1963 atmospheric testing moratorium.

For our experiments the box model was initialized in AD1500 using reconstructed atmospheric $\Delta^{14}C$ (Reimer et al., 2013) and allowed to spin-up for 1,000 years. It was then run forward to 1950 using IntCal13 (Reimer et al., 2013) as the atmospheric $\Delta^{14}C$ forcing. In 1950 it was then forced with the mid-latitude northern hemisphere $\Delta^{14}C$ composite of Hua et al., (2013), which is dominated by the atmospheric data of Levin and Kromer (2004) and Levin et al., (2013). The manually derived best-fit to the NPSG surface ocean prepostbomb transition reconstructions (Figure 5), while meeting the deep Pacific $\Delta^{14}C$ requirement, requires a ~30% higher gas exchange (25 vs. 19 mole-m^{-2}-yr^{-1}) relative to the reference curve of Stuiver et al. (1983), and a K_z that is increased by ~10% (1.4 vs. 1.26 cm^{-2}-s^{-1}). A similarly high gas exchange rate is required

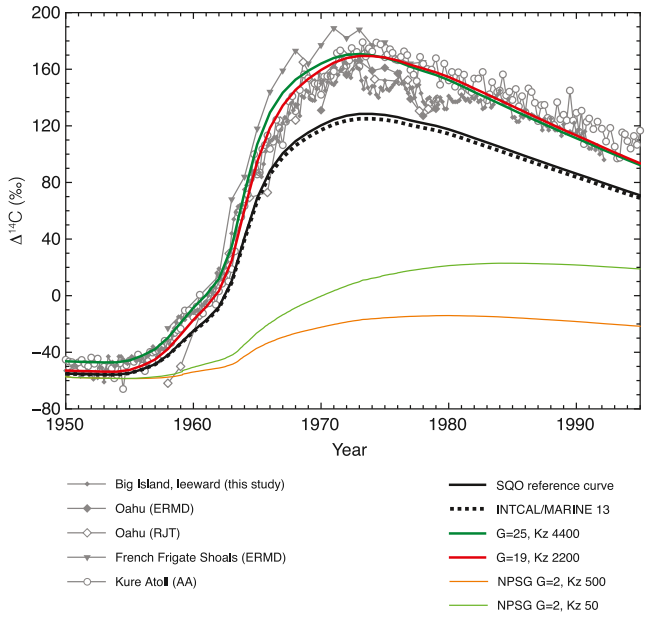

Figure 5. Reconstructed surface water $\Delta^{14}C$ for the subtropical gyre (symbols as in Figure 2, but as greyscale) and that predicted with a 1-D box diffusion model. No bias correction has been applied to match prebomb surface $\Delta^{14}C$ values. The standard "SQO" model estimate (black solid line: K_z 3,970 m^2-yr^{-1} equivalent to 1.26 cm^2-s^{-1} and G 19 mol-m^{-2}-yr^{-1}) is consistent with that of Stuiver et al. (1983). The Marine13 estimate (dotted black line: Reimer et al., 2013) has a slightly larger K_z 4,220 m^2-yr^{-1} (1.34 cm^2-s^{-1}), but the same 19 mol-m-$^2s^{-1}$ gas flux. This K_z was selected to best capture the Holocene surface $\Delta^{14}C$ inferred from Th/U and ^{14}C dated corals. With a constraint to match deep Pacific $\Delta^{14}C$, to capture the observed prepost bomb transition (thick red line) G is increased to 25 mol-m^2-yr^{-1} and K_z to 4,400 (1.4 cm^2-s^{-1}). Relaxing the deep ocean constraint, but matching interior prebomb Δ ^{14}C at 400–500 m (~-100‰) and keeping G at 19 mol-m^{-2}-yr^{-1}, requires a K_z of 2,200, equivalent to 0.62 cm^2-s^{-1} (thick green line). The local and regional air-sea CO_2 exchange is much smaller, 1–2 mol-m^2-yr^{-1}, than the global G. The multidecadal K_z for the mid-latitude North Pacific subthermocline water (26.4–26.7 σt) is <630 m^2-yr^{-1}. We represent the regional low K_z as 500 (thin red line) and 50 (thin green line) m^2-yr^{-1}.

to capture the postbomb reconstructed surface water $\Delta^{14}C$ history of the Sargasso Sea (not shown). The combination of higher G and K_z does yield a slightly more positive deep Pacific (−160‰) $\Delta^{14}C$.

The required G, and its corollary k, the gas transfer or piston velocity, are higher than those inferred from a global ocean inventory of bomb-^{14}C (e.g., Sweeney et al., 2007; Wanninkhof et al., 2009 and references therein) but similar to 1-D estimates for other surface-^{14}C reconstructions (e.g., Chakraborty et al., 1994; Fallon et al., 2003). Reconstructed winds for Hawaii (DaSilva et al., 1994) are not significantly different during the rise in atmospheric ^{14}C relative to the climatological mean. Higher velocity winds, in addition to increasing bubble injection and breaking waves, would result in more air-sea exchange of the bomb transient. We interpret our high G requirement to be a consequence of attempting to reconstruct the "short-term" (few decades) regional response of surface $\Delta^{14}C$ where only shallow densities in the gyre, approaching 25.0 sigma_t, are directly ventilated.

If this interpretation is correct, and under this presumption, we can relax the constraint on deep Pacific radiocarbon values. While keeping G fixed at 19 mole-m^{-2}-yr^{-1} a good fit to the coral-based $\Delta^{14}C$ reconstructions is with a K_z = 2,000m^2-yr^{-1} or 0.62 cm^2-s^{-1} (Figure 5). Although released from the constraint of deep Pacific $\Delta^{14}C$, this K_z and G provides a reasonable fit to prebomb $\Delta^{14}C$ observations in deep-sea corals from the NPSG at the top of the mesopelagic, 400–500m water depth, where $\Delta^{14}C$ is ~−100‰ (Roark et al., 2006).

A challenge with this approach is we know the mean local-regional NPSG air-sea CO_2 flux is not 19–20 mole-m^{-2}-yr^{-1}. The local-regional piston velocity using the most recent Wanninkhof (2014) formulation is ~16cm-hr^{-1} but the air-sea CO_2 gradient is small, ~18 μatm (e.g., Keeling et al., 2004). The small air-sea CO_2 gradient leads to a small air-sea exchange, which locally is ≤1 mole-m^2-yr^{-1} (Keeling et al., 2004) and regionally 1–2 mole-m^2-yr^{-1} (Ishii et al., 2014; Sutton et al., 2017). The multidecadal K_z for the mid-latitude North Pacific subthermocline waters in the 26.4–26.7 density range derived from argon supersaturation (Emerson et al., 2012), is quite small: <0.2 cm^2-s^{-1} (<630 m^2-yr^{-1}) and akin to the K_z estimated by deliberate tracer release experiments (e.g., Ledwell et al., 1998 among many subsequent experiments). We highlight these boundary conditions in the 1-D model where we set the prebomb surface and ocean profile by initially forcing the model with global conditions (G 19 mole-m^2-yr^{-1}, K_z 4,220 m^2-yr^{-1}) and then, in 1954, change G to 2 mole-m^2-yr^{-1} and K_z to 500 or 50 m^2-yr^{-1}. Under these conditions, the simple 1-D box diffusion model cannot recreate the main features of the pre/postbomb surface $\Delta^{14}C$ history (Figure 5). Dropping K_z to 1 m^2-yr^{-1}, in an attempt to "pile-up" bomb-^{14}C in the surface water, has the desired effect of increasing the prepostbomb $\Delta^{14}C$ amplitude ($\Delta\Delta^{14}C$), but the increase is continuous to present without any distinct "peak." The only means in the 1-D box model to shift the year of the peak surface ocean $\Delta^{14}C$, and at the same time have a realistic pre/postbomb $\Delta\Delta^{14}C$ amplitude is to increase the flux (G) or significantly decrease the mixed layer depth (see also Duffy et al., 1995 for a similar interpretation of coarse OGCMs). One possible implication of this observation is there is a strong influence of waters recirculated within the NPSG, from the northern edge of the gyre with much higher mean winds and uptake of CO_2 (cf., Figure 5, Ishii et al., 2014), but with similar surface water $\Delta^{14}C$ values, on the overall shape and amplitude of the NPSG ^{14}C surface water history. The several month equilibration timescale of CO_2 means that surface waters recirculating within the NPSG, even if in near equilibrium with atmospheric pCO_2, a disequilibrium isotope flux can continue to move bomb-^{14}C into surface waters. A related aspect could be that short duration high wind velocity (and assumed air-sea

CO_2 and isotope exchange) events, such as storms and typhoons, have an outsized influence on air-sea isotope exchange.

6. Conclusions

We have reconstructed the surface water $\Delta^{14}C$ history over the time interval 1947–1992 in the subtropical North Pacific as recorded in a coral from the lee of the Big Island of Hawai'i. Prebomb values are approximately −55‰ (±1, SE of the mean) and exhibit seasonal and interannual variations consistent with wind driven, winter mixing and lateral exchange. The postbomb maximum occurs in 1971 with a mean annual value of 160‰. The $\Delta^{14}C$ time-series reflects both local and regional circulation features with spectral peaks in the ENSO band (3–5 years), in addition to a strong annual signal. After the postbomb maximum and for the duration of our reconstruction, surface water $\Delta^{14}C$ did not decrease monotonically but has inflection points coincident with La Niña events following moderate to strong El Niños. This highlights the advection and mixing of lower $\Delta^{14}C$ water from the tropics and the California Current System into the NPSG. A direct comparison of the postbomb $\Delta^{14}C$ record and that of climate indices (e.g., Niño3) is complicated due to the transient nature and penetration of bomb-^{14}C into the subsurface, which obviates the quasi steady-state situation where subthermocline waters have lower $\Delta^{14}C$ values relative to surface values and a direct scaling to the intensity of ENSO anomalies.

Data Availability Statement

Data presented in this manuscript will be archived at NOAA/NCEI Paleoclimate (https://www.ncdc.noaa.gov/data-access/paleoclimatology-data/datasets/coral-sclerosponge), and the Queen's University, Belfast (QUB) marine ^{14}C database (calib.org). The KUA-1 coral cores will be archived at the American Museum of Natural History, New York, NY.

Acknowledgments
Coral cores were collected and supplied by Eric Cathcart, Sarah Gray, Gordon Tribble, and Sheila Griffin. Ethan Goddard supervised milling and all stable isotope and ICP-OES analyses. We thank Brian Frantz, Jessica Westbrook, and Paula Zermeño for pressing targets made by TG. The "Arand" spectral package was maintained and distributed by Phil Howell, Brown University. We are particularly grateful to Keith Rodgers who provided comments, criticisms, and stimulated additional thinking on an early version of this manuscript. The analytical work was supported by grants to T. Guilderson and M. Kashgarian (98ERI002), to D. Schrag from NSF's program in Physical Oceanography (OCE-9796253) and to E. Druffel from NSF's program in Chemical Oceanography (OCE-8915919 and OCE-9314691). Portions of this work were performed under the auspices of the U.S. Department of Energy by the Lawrence Livermore National Laboratory under contracts W-7405-Eng-48 and DE-AC52-07NA27344.

References

Andrews, A. H., Siciliano, D., Potts, D. C., DeMartini, E. E., & Cavarrubias, S. (2016). Bomb radiocarbon and the Hawaiian Archipelago: coral, otoliths, and seawater. *Radiocarbon*, *58*, 531–548.

Bidigare, R. R., Benitez-Nelson, C., Leonard, C. L., Quay, P. D., Parsons, M. L., Foley, D. G., & Seki, M. P. (2003). Influence of a cyclonic eddy on microheterotroph biomass and carbon export in the lee of Hawai'i. *Geophysical Research Letters*, *30*. https://doi.org/10.1029/2002GL016393

Bingham, F. M., & Lukas, R. (1996). Seasonal cycles of temperature, salinity and dissolved oxygen observed in the Hawaii Ocean Time-series. *Deep-Sea Research Part II*, *43*, 199–213.

Broecker, W. S., & Peng, T. H. (1982). *Tracers in the sea* (p. 689). Palisades, NY: ELDIGO Press.

Brown, T. A., Farwell, G. W., Grootes, P. M., Schmidt, F. H., & Stuiver, M. (1993). Intra-annual variability of the radiocarbon content of corals from the Galapagos Islands. *Radiocarbon*, *35*, 245–251.

Chakraborty, S., Ramesh, R., & Krishnaswami, S. (1994). Air-sea exchange of CO2 in the Gulf of Kutch, northern Arabian Sea based on bomb-carbon in corals and tree rings. *Proceedings of the Indiana Academy of Science*, *103*, 329–340.

Chu, P. S., & Chen, H. (2005). Interannual and interdecadal rainfall variations in the Hawaiian Islands. *Journal of Climate*, *18*(4), 4796–4813.

Coplen, T. B. (1993). Reporting of stable carbon, hydrogen, and oxygen isotopic abundances. Reference and intercomparison materials for stable isotopes of light elements. In Technical document (Vol. 825, pp. 31–38). Vienna, Austria: International Atomic Energy Agency.

DaSilva, A., Young, C. C., & Levitus, S. (1994). *Atlas of Surface Marine Data 1994*, 1-5, Washington, DC: NOAA.

Deser, C., Alexander, M. A., & Timlin, M. S. (1996). Upper-ocean thermal variations in the North Pacific during 1970-1991. *Journal of Climate*, *9*(1), 1840–1855.

Diaz, H. F., & Giambelluca, T. W. (2012). Changes in atmospheric circulation patterns associated with high and low rainfall regimes in the Hawaiian Islands region on multiple time scales. *Global and Planetary Change*, *98–99*, 97–108.

Dodge, R. E., Vaisnys, J. R., Rhoads, D. C., & Lutz, R. A. (1980). Skeletal growth chronologies of recent and fossil corals. In *Skeletal growth of aquatic organisms, topic in geobiology* (pp. 493–517). New York, NY: Plenum.

Doney, S.C., Lindsay, K., Caldeira, K., Campin, J. M., Drange, H., Dutay, J. C., et al. (2004). Evaluating global ocean carbon models: the importance of realistic physics. *Global Biogeochemical Cycles*, *18*, GB3017. https://doi.org/10.1029/2003GB002150,2004

Druffel, E. R. M. (1987). Bomb radiocarbon in the Pacific: Annual and seasonal timescale variations. *Journal of Marine Research*, *45*, 667–698.

Druffel, E. R. M., Griffin, S., Glynn, D. S., Dunbar, R. B., Mucciarone, D. A., & Toggweiler, J. R. (2014). Seasonal radiocarbon and oxygen isotopes in a Galapagos coral: Calibration with climate indices. *Geophysical Research Letters*, *41*, 5099–5105. https://doi.org/10.1002/2014GL060504

Druffel, E. R. M., Griffin, S., Guilderson, T. P., Kashgarian, M., Southon, J., & Schrag, D. P. (2001). Changes in subtropical North Pacific radiocarbon and their correlation with climate variability. *Radiocarbon*, *43*, 15–25.

Duffy, P. B., Eliason, D. E., Bourgois, A. J., & Covey, C. C. (1995). Simulation of bomb radiocarbon in two global general circulation models. *Journal of Geophysical Research*, *100*(22), 22545–22564.

Emerson, S., Ito, T., & Hamme, R. C. (2012). Argon supersaturation indicates low decadal-scale vertical mixing in the ocean thermocline. *Geophysical Research Letters*, *39*, L18610. https://doi.org/10.1029/2012GL053054

Fairbanks, R. G., & Dodge, D. (1979). Annual periodicity of the 18O/16O and 13C/12C ratios in the coral Montastrea annularis, *Geochimica et Cosmochimica Acta*, *43*, 1009–1020.

Fallon, S. J., Guilderson, T. P., & Caldeira, K. (2003). Carbon isotope constraints on vertical mixing and air-sea CO2 exchange. *Geophysical Research Letters*, *30*, 2289. https://doi.org/10.1029/2003GL018049

Fine, R. A., Maillet, K. A., Sullivan, K. F., & Willey, D. (2001). Circulation and ventilation flux of the Pacific Ocean. *Journal of Geophysical Research*, *106*(C10), 22159–22178.

Flament, P. (1996). *The ocean atlas of Hawai'i*. Honolulu, HI: School of Ocean and Earth Science and Technology, University of Hawai'i. https://www.pacioos.hawaii.edu/education/ocean-atlas/

Follows, M. J., Ito, T., & Marotzke, J. (2002). The wind-driven, subtropical gyres and atmospheric pCO_2. *Global Biogeochemical Cycles*, *16*, 601–609. https://doi.org/10.1029/2001GB0017

Gove, J. M., Williams, G. J., McManus, M. A., Heron, S. F., Sandin, S. A., Vetter, O. J., & Foley, D. G. (2013). Quantifying Climatological ranges and anomalies for Pacific coral reef ecosystems. *PloS One*, *8*(4), e61974. https://doi.org/10.1371/journal.pone.0061974

Graven, H. D., Gruber, N., Key, R., Khatiwala, S., & Giraud, X. (2012). Changing controls on oceanic radiocarbon: new insights on shallow-to-deep ocean exchange and anthropogenic CO2 uptake. *Journal of Geophysical Research*, *117*, C10005. https://doi.org/10.1029/2012JC008074

Grottoli, A. (1999). Variability of stable isotopes and maximum linear extension in reef-coral skeletons at Kaneohe Bay, Hawaii. *Marine Biology*, *135*, 437–449.

Guilderson, T. P., Caldeira, K., & Duffy, P. B. (2000). Radiocarbon as a diagnostic tracer in ocean and carbon cycle modeling. *Global Biogeochemical Cycles*, *14*, 887–902.

Guilderson, T. P., & Schrag, D. P. (1998). Abrupt shift in subsurface temperatures in the Eastern Tropical Pacific associated with recent changes in El Niño. *Science*, *281*, 240–243.

Guilderson, T. P., Schrag, D. P., Kashgarian, M., & Southon, J. (1998). Radiocarbon Variability in the Western Equatorial Pacific inferred from a high-resolution coral record from Nauru Island. *Journal of Geophysical Research*, *103*(2), 24641–24650.

Gu, D., & Philander, S. G. H. (1997). Interdecadal climate fluctuations that depend on exchanges between the tropics and extratropics. *Science*, *275*, 805–807.

Holte, J., & Talley, L. (2009). A new algorithm for finding mixed layer depths with applications to Argo data and sub Antarctic mode water formation. *Journal of Atmospheric and Oceanic Technology*, *26*, 1920–1939.

Hua, Q., Barbetti, M., & Rakowski, A. Z. (2013). Atmospheric Radiocarbon for the Period 1950-2010. *Radiocarbon*, *56*, 2059–2072.

Ingram, B. L., & Southon, J. (1996). Reservoir ages in Eastern Pacific coastal and estuarine waters. *Radiocarbon*, *38*, 573–582.

Ishii, M., Feely, R. A., Rodgers, K. B., Park, G.-H., Wanninkhof, R., Sasano, D., et al. (2014). Air-sea CO2 flux in the Pacific Ocean for the period 1990-2009. *Biogeosciences*, *11*, 709–734. https://doi.org/10.5194/bg-11-709-2014

Ito, T., & Follows, M. J. (2003). Upper ocean control on the solubility pump of CO2. *Journal of Marine Research*, *61*, 465–489.

Iudicone, D., Rodgers, K. B., Plancherel, Y., Aumont, O., Ito, T., Key, R. M., et al. (2016). The formation of the ocean's anthropogenic carbon reservoir. *Scientific Reports*, *6*, 35473. https://doi.org/10.1038/srep35473

Jenkins, W. J. (1996). *Studying thermocline ventilation and circulation using tritium and 3He*. Paper presented at Maurice Ewing Symposium "Application of Trace Substance Measurements to Oceanographic Problems. AGU, Washington, DC.

Johnson, G. C., & McPhaden, M. J. (1999). Interior pycnocline flow from the subtropical to the Equatorial Pacific Ocean. *Journal of Physical Oceanography*, *29*, 3073–3089.

Keeling, C. D., Brix, H., & Gruber, N. (2004). Seasonal and long-term dynamics of the upper ocean carbon cycle at Station ALOHA near Hawaii. *Global Biogeochemical Cycles*, *18*, GB4006. https://doi.org/10.1029/2004GB002227

Kerr, L. A., Andrews, A. H., Munk, K., Coale, K. H., Frantz, B. R., Cailliet, G. M., & Brown, T. A. (2005). Age validation of quillback rockfish (Sebastes maliger) using bomb radiocarbon. *Fisheries Bulletin*, *103*, 97–107.

Key, R. M., Quay, P. D., Jones, G. A., McNichol, A. P., vonReden, K. F., & Schneider, R. J. (1996). WOCE AMS Radiocarbon I: Pacific Ocean results (P6, P16 and P17). *Radiocarbon*, *38*, 425–518.

Khatiwala, S., Tanhua, T., Mikaloff Fletcher, S., Gerber, M., Gerber, S. C., Graven, H. D., et al. (2013). Global ocean storage of anthropogenic carbon. *Biogeosciences*, *10*, 2169–2191.

Laurindo, L. C., Mariano, A. J., & Lumpkin, R. (2017). An improved near-surface velocity climatology for the global ocean from drifter observations. *Deep-Sea Research Part I*, *124*, 73–92.

Ledwell, J. R., Watson, A. J., & Law, C. S. (1998). Mixing of a tracer in the pycnocline. *Journal of Geophysical Research*, *103*(C10), 21499–21529.

Levin, I., & Kromer, B. (2004). The tropospheric 14CO2 level in mid-latitudes of the Northern Hemisphere (1959-2003). *Radiocarbon*, *46*, 1261–1272.

Levin, I., Kromer, B., & Hammer, S. (2013). Atmospheric D14CO2 trend in Western European background air from 2000 to 2012. *Tellus B: Chemical and Physical Meteorology*, *65*, 20092. https://doi.org/10.3402/tellusb.v65i0.20092

Lumpkin, R., & Johnson, G. C. (2013). Global ocean surface velocities from drifters: Mean, variance, El Niño-Southern Oscillation response, and seasonal cycle. *Journal Geophysical Research-Oceans*, *118*(2), 2992–3006.

Mahadevan, A. (2001). An analysis of bomb radiocarbon trends in the Pacific. *Marine Chemistry*, *73*, 273–290.

Matsumoto, K., Sarmiento, J. L., Key, R. M., Aumont, O., Bullister, J. L., Caldeira, K., et al. (2004). Evaluation of ocean carbon cycle models with data-based metrics. *Geophysical Research Letters*, *31*, L07303. https://doi.org/10.1029/2003GL018970

McConnaughey, T. A., Burdett, J., Whelan, J. F., & Paull, C. K. (1997). Carbon isotopes in biological carbonates: Respiration and photosynthesis. *Geochimica et Cosmochimica Acta*, *61*, 611–622.

Monterey, G. I., & Levitus, S. (1997). Seasonal variability of mixed layer depth for the world ocean, NOAA NESDIS Atlas (Vol. 14), 100 pp. Washington, DC: U.S. Gov. Printing Office.

Moore, M. D., Schrag, D. P., & Kashgarian, M. (1997). Coral radiocarbon constraints on the source of the Indonesian throughflow. *Journal of Geophysical Research*, *102*(12), 12359–12365.

Oeschger, H., Siegenthaler, U., Schotterer, U., & Gugelmann, A. (1975). A box diffusion model to study carbon dioxide exchange in nature. *Tellus B: Chemical and Physical Meteorology*, *27*, 168–192.

Orr, J. C., Reimer, E. M., Mikolajewicz, U., Monfray, P., Sarmiento, J. L., Toggweiler, J. R., et al. (2001). Estimates of anthropogenic carbon uptake from four three-dimensional global ocean models. *Global Biogeochemical Cycles*, *15*(1), 43–60.

Östlund, H. G., & Stuiver, M. (1980). GEOSECS Pacific radiocarbon. *Radiocarbon*, *22*, 25–53.

O'Connor, C. F., Chu, P. S., Hsu, P. C., & Kodama, K. (2015). Variability of Hawaiian winter rainfall during La Niña events since 1956. *Journal of Climate*, *28*(7), 7809–7823.
Qiu, B. (2002). Large-scale variability in the midlatitude subtropical and subpolar North Pacific Ocean: Observations and causes. *Journal of Physical Oceanography*, *32*, 353–375.
Quay, P. D., Stuiver, M., & Broecker, W. S. (1983). Upwelling rates for the equatorial Pacific Ocean derived from the bomb 14C distribution. *Journal of Marine Research*, *41*, 769–792.
Rayner, N. A., Horton, E. B., Parker, D. E., Folland, C. K., & Hackett, R. B. (1996). *Version 2.2 of the global sea-ice and sea surface temperature data set, 1903-1994. CRTN 74*. Bracknell, UK: Hadley Centre, Met Office.
Reimer, P. J., Bard, E., Bayliss, A., Beck, J. W., Blackwell, P. G., Bronk Ramsey, C., et al. (2013). Intcal 13 and Marine13 Radiocarbon age calibration curves 0-50,000 years Cal BP. *Radiocarbon*, *55*, 1869–1887.
Reimer, P. J., Brown, T. A., & Reimer, R. W. (2004). Discussion: Reporting and calibration of post-bomb 14C Data. *Radiocarbon 46*, 1299–1304.
Roark, E. B., Guilderson, T. P., Dunbar, R. B., & Ingram, B. L. (2006). Radiocarbon based ages and growth rates: Hawaiian deep-sea corals. *Marine Ecology Progress Series*, *327*, 1–14.
Robinson, M. K. (1969). Theoretical predictions of subtropical countercurrent confirmed by bathythermograph data. *Bulletin of Japanese Society Fisheries and Oceanography*, 115–121.
Rodgers, K. B., Schrag, D. P., Cane, M. A., & Naik, N. H. (2000). The bomb 14C transient in the Pacific Ocean. *Journal of Geophysical Research*, *105*(C4), 8489–8512.
Schrag, D. P. (1999). Rapid analysis of high-precision Sr/Ca ratios in corals and other marine carbonates. *Paleoceanography*, *14*, 97–102.
Shen, G. T., Linn, L. J., Campbell, T. M., Cole, J. E., & Fairbanks, R. G.. 1992. A chemical indicator of trade wind reversal in corals from the western tropical Pacific. *Journal of Geophysical Research*, *97*, 12689–12697.
Stuiver, M., Pearson, G. W., & Brazunias, T. (1986). Radiocarbon age calibration of marine samples back to 9000 cal yr BP. *Radiocarbon*, *28*, 980–1021.
Stuiver, M., & Polach, H. A. (1977). Discussion and reporting of 14C data. *Radiocarbon*, *19*, 355–363.
Stuiver, M., Quay, P. D., & Östlund, G. H. (1983). Abyssal water carbon-14 distribution and the age of the world oceans. *Science*, *18*, 849–851.
Sutton, A. J., Wanninkhof, R., Sabine, C. L., Feely, R. A., Cronin, M. F., & Weller, R. A. (2017). Variability and trends in surface water pCO_2 and CO_2 flux in the Pacific Ocean. *Geophysical Research Letters*, *44*, 5627–536. https://doi.org/10.1002/2017GL073814
Sweeney, C., Gloor, E., Jacobson, A. R., Key, R. M., McKinley, G., Sarmiento, J. L., & Wanninkhof, R. (2007). Constraining global air-sea gas exchange for CO2 with recent bomb 14C measurements. *Global Biogeochemical Cycles*, *21*, GB2015. https://doi.org/10.1029/2006GB002784
Toggweiler, J. R., Dixon, K., & Broecker, W. S. (1991). The Peru upwelling and the ventilation of the South Pacific thermocline. *Journal of Geophysical Research*, *96*, 20467–2097.
Toggweiler, J. R., Dixon, K., & Bryan, K. (1989). Simulations of radiocarbon in a coarse-resolution world ocean model I: steady state prebomb distributions. *Journal of Geophysical Research*, *94*(C6), 8217–8242.
Vogel, J. S., Southon, J. R., & Nelson, D. E. (1987). Catalyst and binder effects in the use of filamentous graphite for AMS. *Nuclear Instruments & Methods in Physics Research, Section B*, *29*, 50–56.
Wanninkhof, R. (1992). Relationship between gas exchange and wind speed over the ocean. *Journal of Geophysical Research*, *97*, 7373–7381.
Wanninkhof, R. (2014). Relationship between wind speed and gas exchange over the ocean revisited. *Limnology and Oceanography: Methods*, *12*, 351–362.
Wanninkhof, R., Asher, W. E., Ho, D. T., Sweeney, C., & McGillis, W. R. (2009). Advances in quantifying air-sea gas exchange and environmental forcing. *Annual Reviews in Marine Science*, *1*, 213–244.
Wyrtki, K., & Kilonsky, B. (1984). Mean water and current structure during the Hawaii to Tahiti shuttle experiments. *Journal of Physical Oceanography*, *14*, 242–254.
Yoshida, S., Qiu, B., & Hacker, P. (2010). Wind generated eddy characteristics in the lee of the island of Hawaii. *Journal of Geophysical Research*, *115*, C03019. https://doi.org/10.1029/2009JC005417
Zhang, R. H., Rothstein, L. M., & Busalacchi, A. J. (1998). Origin of upper-ocean warming and El-Nino changes in the tropical Pacific Ocean. *Nature*, *391*, 879–883.